Journal of
Composites Science

MDPI

Article

An Eco-Friendly, Simple, and Inexpensive Method for Metal-Coating Strontium onto Halloysite Nanotubes

Anusha Elumalai [1] and David K. Mills [1,2,*]

[1] Molecular Science and Nanotechnology, Louisiana Tech University, Ruston, LA 71272, USA
[2] School of Biological Sciences, Louisiana Tech University, Ruston, LA 71272, USA
* Correspondence: dkmills@latech.edu; Tel.: +1-318-267-5644; Fax: +1-318-257-4574

Abstract: Osteoporosis increases the risk of bone fracture by reducing bone mass and thereby increasing bone fragility. The addition of strontium (Sr) nanoparticles in bone tissue results in a strengthening of the bone, induction bone formation by osteoblasts, and reduction of bone reabsorption by osteoclasts. The use of Sr for bone tissue regeneration has gained significant research interest in recent years due to its beneficial properties in treating osteoporotic-induced bone loss. We hypothesized that Sr-coated and antibiotic-doped HNTs could be used in antimicrobial coatings and as an antibacterial drug delivery vehicle. Accordingly, we coated HNTs with strontium carbonate (SrHNT) using a simple, novel, and effective electrodeposition method. We tested the antibacterial properties of SrHNT on *Escherichia coli*, *Staphylococcus aureus*, and *Staphylococcus epidermis* using the disc diffusion method. We assessed the potential cytotoxic and proliferative effects of SrHNTs on pre-osteoblasts using a Live/Dead cytotoxicity and cell proliferation assay. We successfully coated HNTs with strontium using a one-step benign coating method that does not produce any toxic waste, unlike most HNT metal-coating methods. Antibacterial tests showed that the SrHNTs had a pronounced growth inhibition effect, and cell culture studies using MC 3T3 cells concluded that SrHNTs are cytocompatible and enhance cell proliferation.

Keywords: 3D printing; antibacterial; drug delivery; halloysite nanotubes; nanotechnology; surface modification; tissue regeneration

Citation: Elumalai, A.; Mills, D.K. An Eco-Friendly, Simple, and Inexpensive Method for Metal-Coating Strontium onto Halloysite Nanotubes. *J. Compos. Sci.* **2022**, *6*, 276. https://doi.org/10.3390/jcs6090276

Academic Editor: Konda Gokuldoss Prashanth

Received: 16 July 2022
Accepted: 8 September 2022
Published: 17 September 2022

1. Introduction

The long recovery time required for healing bone defects in many patients suggests the need for a superior osteogenic scaffold [1,2]. Osteomyelitis is a refractory and challenging condition, often requiring multiple surgical interventions, and can lead to limb amputation or even death [3–5]. Chronic osteomyelitis is remarkably impactful on the elderly [5,6]. Disadvantages of the polymethyl-methacrylate (PMMA) carriers currently used include insufficient antibiotic release, lack of sustained release, and the need for surgical removal of PMMA beads, as they are not biodegradable [6,7]. In contrast, biodegradable and polymeric antibiotic carriers can offer a sustained release, eliminating the need for removal until they are gradually replaced by new tissue [8–10].

Osteoporosis increases the risk of bone fracture, resulting from decreased bone mass and increased bone fragility [11]. This disorder affects all ages, with 10 million Americans are currently afflicted and another 34 million are at risk [12,13]. With an aging population, the incidence of osteoporosis arising from various causes leads to high bone turnover and a reduction in bone material properties [12,13]. Currently, over two million fractures occur each year, costing over $19 billion, and figure will rise to 3 million fractures per year by 2025, with costs estimated at $25 billion per year [13,14]. Bone defects are a leading cause of morbidity and disability in elderly patients, and this number will increase as 'Baby Boomers' retire [14]. Currently, there are over 200,000 hip replacements performed in the US each year. This number will rise due to increased life expectancies, more active lifestyles, and a larger population of at-risk individuals [13,14].

Strontium (Sr) has received much attention in recent years due to its ability to promote bone formation [15]. Specifically, Sr has been shown to increase osteoblast replication, differentiation, and bone matrix mineralization, as well as to reduce osteoclast differentiation and bone reabsorption [16–18]. Sr has also been reported to induce mesenchymal stem cell (MSC) commitment to the osteoblastic lineage [19]. The in-situ release of Sr at a proper dosage, directly at the implant–tissue interface or bone defect site, has been proposed to enhance the implant osseointegration and new bone formation [20–22]. Sr nanoparticles have been incorporated into hydroxyapatite (HA) [23], tricalcium phosphate (TCP) [24], and calcium phosphate cement (CPC) [25]. In these materials, Sr was shown to induce osteoblasts' bone formation, [26] reduce osteoclastic activity, and initiate apoptosis [27,28]. Thus, incorporating Sr into a bone implant is an attractive method for developing a superior osteogenic scaffold.

Halloysite nanotubes (HNTs) are aluminosilicates that are quite chemically similar to kaolin clay. HNTs have a length ranging from 200 to 1500 nm, with an average length of 1000 nm [29]. The inner lumen has a diameter of 15 $\pm$ 2 nm, and the tube has an overall average diameter of 50 nm. The widespread use of HNTs is due to their biocompatibility, bioactivity, durability, availability, and low cost [29,30]. Unlike kaolin, instead of flat "sheets", HNTs are rolled into multilayered tubes [29,30]. The outer silica surface "gains" a negative charge in rolling, while aluminum's inner surface holds a positive charge [30]. This polarization of the tube allows for functional engineering, surface modification by various methods [31], or the prolonged-release profiles of loaded materials [32]. Initial studies on HNTs have found improved strength properties when they are added to other materials, such as epoxy, polymers, and paper [33–35]. Antibiotics, drugs, and growth factors have all been successfully loaded into the lumen of HNTs [36–38]. Previous studies from our lab have indicated that HNTs have potent osteogenic and chemotactic properties [39–42]. Alginate and HNT hydrogel nanocomposites have shown a pronounced osteogenic effect on seeded osteoblasts. Moreover, microscopic observations suggested that osteoblasts migrated and clustered around the HNTs and doped HNTs [41,42]. The potential of HNTs and BMP-2-doped HNTs to serve as a chemoattractant for pre-osteoblasts was the focus of a more recent study [43]. Here, we measured pre-osteoblast migration in response to the presence of HNTs and HNTs doped with bone morphogenetic protein-2 (BMP-2). Pre-osteoblasts were 'seeded' into collagen gel cultures and assessed for their ability to attract pre-osteoblasts and produce an osseous matrix. The presence of HNTs stimulated cell migration. The highest migration rate of osteoblasts occurred when the concentration of HNTs was between 100–250 μg/mL [43]. HNTs, in conjunction with a BMP-2, promoted pre-osteoblast cell migration. This suggests that HNTs, when added to a hydrogel, CPC bone cement, or other polymer, may be a means to induce bone and tissue repair in clinical patients.

When CPC/HNT composites doped with dexamethasone (DEX) were added to MSC cultures and observed for alkaline phosphatase activity, it was predicted that composites with DEX-loaded HNTs would promote MSC differentiation; however, the results were unexpected. Differentiation was significantly enhanced on composites containing undoped HNTs, while DEX-loaded HNTs produced insignificant results [39,40], supporting the concept that HNTs inherently have osteogenic potential.

Several methods exist for the surface modification of halloysite nanotubes with metals. Metal acetate and metal salts are substances used to deposit metals on the surface of HNTs, which possess a negative charge [44,45]. Various technologies have been developed that use specific metal compounds and multi-step chemical reactions [45,46]. Many of the current HNT-metallization strategies use halloysite as a metal catalyst support. For example, palladium nanoparticle deposition was achieved through a multi-step reaction with sodium tetrachloride palladate (Na2PdCl4), methanol, and poly (vinyl pyrrolidone) [46]. Halloysite-coated cobalt coatings were achieved by calcinating halloysite and cobalt nitrite under temperatures as high as 623 K [47]. The deposition of silver onto HNTs has included the in situ reduction of silver nitrite through the polyol process [48]. Synthesis of silver within

the HNT inner lumen was achieved by vacuum loading of silver acetate followed by high-temperature calcination [49]. Additionally, methods have shown that iron and nickel can be deposited on the HNT surface through mixing of metal compounds and calcination at high temperatures [50]. These HNT–metal fabrication methods rely on multi-step processing with metal compounds, chemicals, and high temperatures for metallic deposition.

As HNTs are proven nanocarriers with properties that support bone tissue formation, we developed a method for coating HNTs with metal carbonate compounds as the metal ion donor and NMR shift reagents—through a simple breakdown of the salt in water. This method produces a free positively charged metal ion that can readily bind to the negatively charged HNT exterior, resulting in metallic coatings forming on the HNT surface.

The antibacterial properties of SrHNT on three bacterial species, *Escherichia coli, Staphylococcus aureus*, and *Staphylococcus epidermis,* were assessed using the disc diffusion method. In addition, SrHNT's potential cytotoxic effects on mouse pre-osteoblasts (MC3T3-E1) and mouse bone-marrow-derived mesenchymal stem cells (ATCC® Crl-12424™) were studied using Live/Dead cytotoxicity and an MTS cell proliferation assay. The results indicate that HNTs were successfully coated with strontium using a 'green' one-step coating method. This method does not produce any toxic waste, unlike most HNT metal-coating methods. SrHNT was also effective in controlling bacterial growth in all three species studied. Furthermore, cell studies also conclude that SrHNTs were cytocompatible after SrHNT exposure and showed enhanced cell proliferation.

2. Materials

Halloysite and gentamicin were purchased from Sigma Aldrich, St Louis, MO, USA. Cell culture and lab plastics were obtained from MidSci, St. Louis, MO, USA. Alpha minimal essential medium (α-MEM) and Dulbecco's DMEM were obtained from GIBCO Invitrogen, Grand Island, NE, USA. Fetal bovine serum and penicillin were purchased from Phenix Research Products (Candler, Buncombe, NC, USA). TryplE, an animal-free trypsin substitute, and trypan blue were obtained from GIBCO Invitrogen, (Grand Island, NE, USA). Mouse pre-osteoblast MC3T3-E1 (ATCC® CRL-2593™) and mesenchymal stem cells (ATCC® Crl-12424™) cell lines were obtained from ATCC (Manassas, VA, USA). All bacteria mediums were purchased from MidSci, St. Louis, MO, USA. *Escherichia coli, Staphylococcus aureus*, and *Staphylococcus epidermis* were gifts from Dr. Rebecca Girono, Biological Science, from Louisiana Tech University (Ruston, LA, USA).

3. Methods

3.1. Preparation of Sr Coated HNTs

Strontium carbonate ($SrCO_3$) and HNTs were added to distilled water in equal amounts (Figure 1). To assist in the even distribution of additives and to prevent agglomeration, the reaction mixture (Rm) was sonicated at regular intervals for a duration of 30 min over 3 days. The Rm was exposed to three different temperatures. One sample was kept at room temperature (25 °C), another in an incubator (60 °C), and the third sample was microwaved until the solution boiled. The precipitate obtained for all samples was washed in citric acid (Ph = 4) to remove excess CO_3^{2-} ions and was then washed in deionized water three times. The precipitate was collected and air-dried.

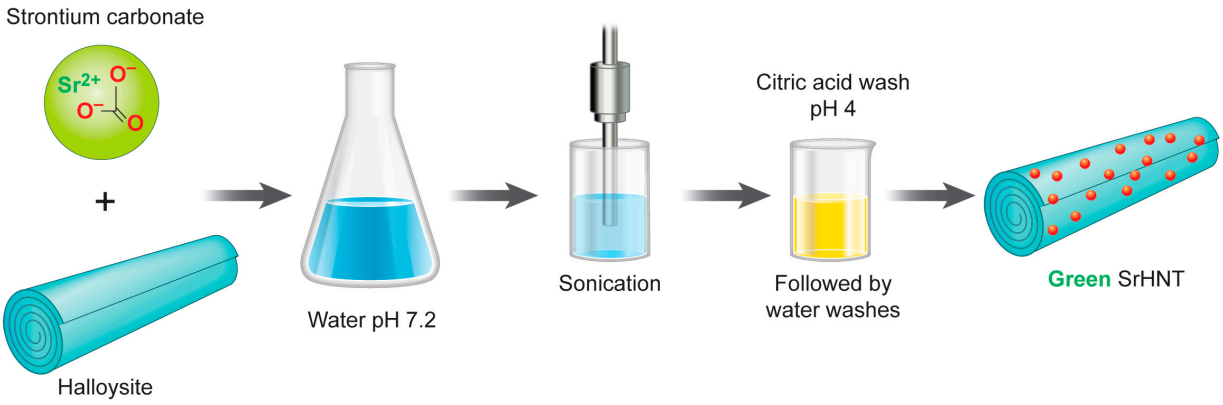

Figure 1. Schematic representation of the process for fabricating SrHNTs.

3.2. Scanning Electron Microscope (SEM)

Samples were prepared for SEM and an S4800 Field Emission SEM, HITACHI was used for imaging of the surface of HNTs. The high magnification obtained by SEM permitted close comparisons of the surface morphologies of the HNT and SrHNTs.

3.3. Energy Dispersive Spectroscopy (EDS)

SEM–EDS analysis was performed for HNTs and SrHNTs using an EDAX dispersive X-ray analyzer attached to a HITACHI S-4800 SEM to evaluate the elemental composition and weight percentage of Sr in the coated HNTs. EDS was conducted at 15 mm with an acceleration voltage of 15 kV and the spectra were analyzed using the EDAX Genesis software.

3.4. X-ray Diffraction (XRD)

XRD for HNT and SrHNT was performed using a Bruker D8 Venture diffractometer (Brunker, Karlsruhe, Germany). The scan speed and step size used were 2 s and 0.02. The diffraction patterns were recorded using a Philips PW 1710 X-ray powder diffractometer over 20 within 3° and 85°.

3.5. Fourier Transformation Infrared (FT-IR) Spectroscopy

FT-IR was performed on HNT, $SrCO_3$, SrHNTs discs, and the discs of groups 1 and 4, to analyze the composition of the powders using the attenuated total reflection (ATR) method. IR spectroscopy is used for the qualitative identification of organic and inorganic compounds. This method was used for confirming the presence of functional groups in organic compounds. The ATR method was selected, as it is a more efficient way to analyze a sample, it provides a more accurate result, and it has a low signal-to-noise ratio.

3.6. Cell Culture

Mouse pre-osteoblast MC3T3-E1 (ATCC® CRL-2593™) and mesenchymal stem cells (ATCC® Crl-12424™) cell lines were obtained from ATCC (Manassas, VA, USA). All cells came cryopreserved from ATCC. Cryovials were thawed and allowed to equilibrate in a water bath; all the cells were cultured in a 25 cm^2 tissue culture flask and incubated at 37 °C under humidified 5% CO_2 and 95% air. Pre-osteoblast and mesenchymal stem cells (MSCs) were incubated in complete alpha-MEM and Dulbecco's modified eagle medium, respectively, containing 10% FBS and 1% penicillin. These two cells lines were chosen to observe if SrHNTs influenced the development of pre-osteoblasts cells towards the osteoblastic lineage and directed MSCs to develop into osteoblasts. Sub-confluent cells were passaged with 0.25% trypsin, collected by centrifugation, suspended in the cell culture medium, and cultured at a 1:4 split into 25 cm^2 tissue culture flasks. All cell lines were passaged to establish a working stock, and, in all experiments, passage four cells were used.

3.7. Viability and Cytotoxicity Testing

A Live/Dead assay kit (Biotium, Fremont, CA, USA) was used to estimate cell viability after exposure to native HNTs and SrHNTs. Cells were seeded into a 48-well plate at a 1×10^5 cells/well concentration and cultured for 24 h. Native HNTs or SrHNTs at concentrations of 0, 25 and 50 µg/mL were added into cell culture plates. The cytotoxicity assay was performed on days 1, 3, 5, and 7. Fluorescence images were taken using an Olympus BX 41 fluorescence microscope fitted with a Nikon digital camera.

3.8. Cell Proliferation Assay

After exposure to native HNTs and SrHNTs, cellular proliferation was assessed using an MTS assay. Native HNTs or SrHNTs at concentrations of 0, 25, and 50 µg/mL were added into cell culture plates. The assessment of cellular proliferation was conducted on days 1, 3, 5, and 7. First, cells were seeded into a 48-well plate at a 1×10^5 cells/well concentration and cultured for 24 h. Next, a 40 µL MTS stock solution was added to each well and cultured for 2 h at 37 °C in darkness. 200 µL of each sample's supernatant were transferred to 96-well plates and read absorbance values at 490 nm by a microplate reader.

3.9. Bacterial Growth Rate Study

The antibacterial properties of HNTs, SrHNTs, and gentamicin-loaded G/HNTs, SrHNTS, and HNTs that were loaded with the drug and then coated with strontium (SrHNT/G). *Escherichia coli* (*E. coli*, ATCC 35218, *Staphylococcus aureus* (*S. aureus,* ATCC BAA-1026), and *Staphylococcus epidermis* (*S. epidermis,* ATCC 14-990) were investigated.

3.10. Micro Titration Method

HNT, SrHNT, G/HNTs, SrHNTs, and SrHNT/G were evaluated for their effect on bacterial growth rate and drug release using the micro-titration method since they were in powder form. The starting concentration of the sample was 10 µg/mL. It was serially diluted in four consecutive wells. Three colony cultures of bacteria (*S. aureus*) were chosen to perform three repetitions of the tests. Bacteria were grown on Luria–Bertani (LB) broth. The test was conducted in Miller–Hilton broth.

3.11. Statistical Analysis

Statistical analysis was performed using Microsoft Excel Analysis ToolPak plugin and Origin 9.6. All experiments were conducted in triplicate, and one-way analysis of variance (ANOVA) with $p < 0.05$ as the significance level was utilized for statistical analysis using SPSS software. Statistically significant data was reported as ($p < 0.05$), and all the results were reported as mean ± standard deviation ($p < 0.05$, $n = 3$) unless otherwise specified.

4. Results

4.1. Fabrication Method for Strontium Coating the Halloysite Surface

Native HNTs were coated with Sr by adding HNTs and strontium carbonate ($SrCO_3$) in identical amounts to distilled water, as seen in Figure 1. A sonicator was used to promote the even distribution of reactants and prevent agglomeration. The reaction mixture (Rm) was sonicated at regular intervals for 30 min over 3 days. The precipitate obtained was then washed in citric acid (Ph = 4) to remove excess CO_3^{2-} ions, and then washed 3 times in distilled water. The precipitate was then collected and dried at room temperature.

4.2. Surface Topography

The coating of Sr on HNT was performed at three different temperatures. The SEM images were taken to confirm the presence of coatings and confirm the best temperature for coatings of the HNTs. The images of the HNTs coated by Sr at room temperature (60 °C) and microwaved were analyzed for successful coating and shown in Figure 2.

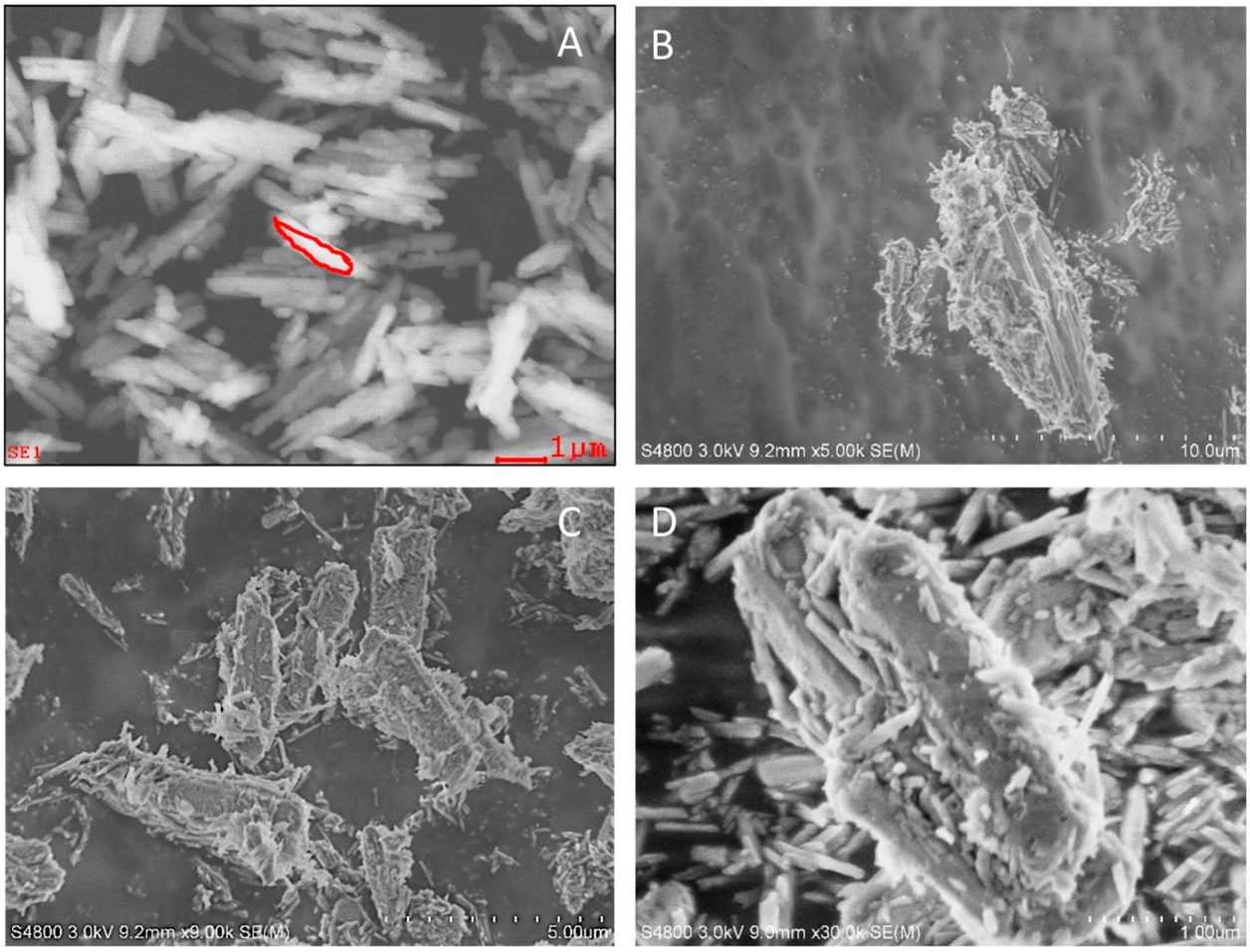

Figure 2. SEM images of HNTs dried under conditions. (**A**) HNT and Sr coated HNTs, (**B**) oven-dried, (**C**) microwaved, (**D**) at room temperature. The red outline is of a single HNT.

As the SEM images show, the coating of Sr was successful in all three exposures. Since the coatings were observed at room temperature, the experiment was conducted three more times to observe the method's consistency. There is an irregular but complete coating of Sr on the HNTs, as seen in Figure 3. HNTs, by default, have a smoother exterior as seen in Figure 2A. The $SrCO_3$ hydrolyze into Sr^{2+} and CO_3^{2-} ions when water is added to the salt.

Since halloysite has a negative exterior surface due to the presence of OH^-, it attracts the positively charged ions to form a bond, which can be either a Van der Waals bond or a weak ionic bond. In both cases, the Sr^{2+} becomes attached to the surface of the HNTs. The bond between Sr^{2+} and HNT surface was not weak since citric acid (pH = 4) was used as a wash to remove the excess CO_3^{2-} ions and the remaining $SrCO_3$ salt. The images were taken after the citric acid was washed away with water. Citric acid was used as a substitute for lemon juice (pH = 2.5) to maintain the pH level's consistency during the washes. Other lemon types possess slightly different properties, which causes procedural variations each time they are used. At lower pH, citric acid is a harmless and non-toxic chemical that provides an environmentally safe option for removal of the excess unwanted ions introduced during the formation of SrHNTs. SEM images showed a successful layering of Sr on HNTs, which formed a bond strong enough to remain stable even after exposure to acid with a pH of 4. This HNT coating and washing method showed that most of the HNTs were coated. The SEM images showed the presence of SrHNT and HNTs.

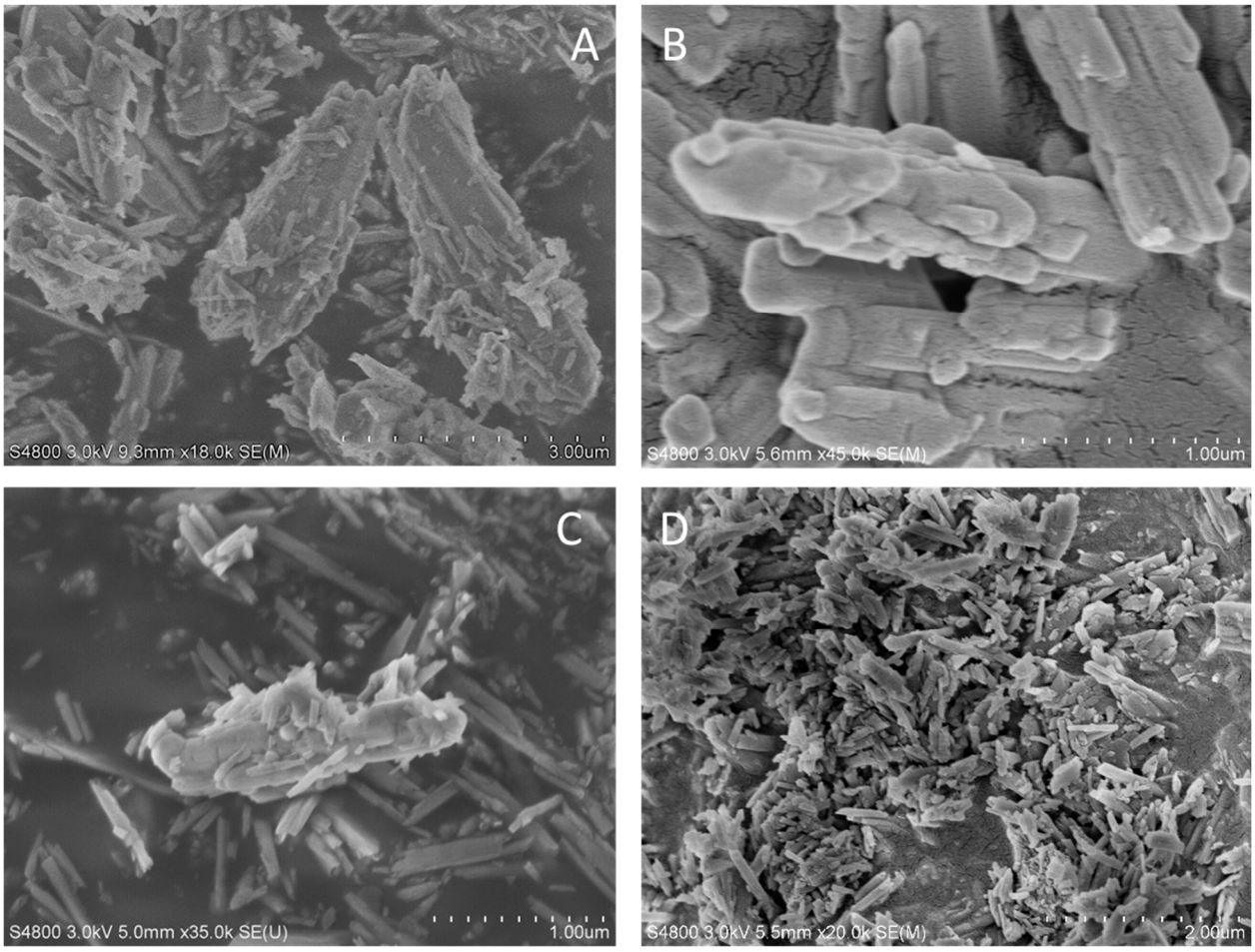

Figure 3. SEM images of SrHNTs of multiple attempts (**A**–**D**) show sediment-like formation on the surface of HNT.

4.3. EDS Analysis

EDS, which is a quantitative analysis of the chemical elements present in a selected region, was performed to ensure Sr's presence on the HNTs. As seen in Figure 4, the EDS–SEM analyzed the chemical characterization of the region selected on HNTs and SrHNTs, as seen in the red outline in Figure 4A,B, respectively.

The quantitative analysis of the different elements presented in the HNT and SrHNT elemental report clearly shows Sr-on-Sr coated HNTs. However, the exact peak of Si is not visible in the reports of SrHNT. Therefore, the value is 0 as the K shell peak of Si overlaps the L shell peak of Sr. All the samples of HNTs and the average of the qualitative compositional information of HNTs and SrHNT are shown in Figure 5.

The presence of the element Sr was confirmed by EDS, giving value to the method of coating SrHNT. The EDS method can be used to determine the presence of a chemical element. It also gives an estimate of their abundance. The accuracy of this method can be affected by various other factors, such as overlapping peaks. For a more accurate estimation of the sample composition, further tests were performed.

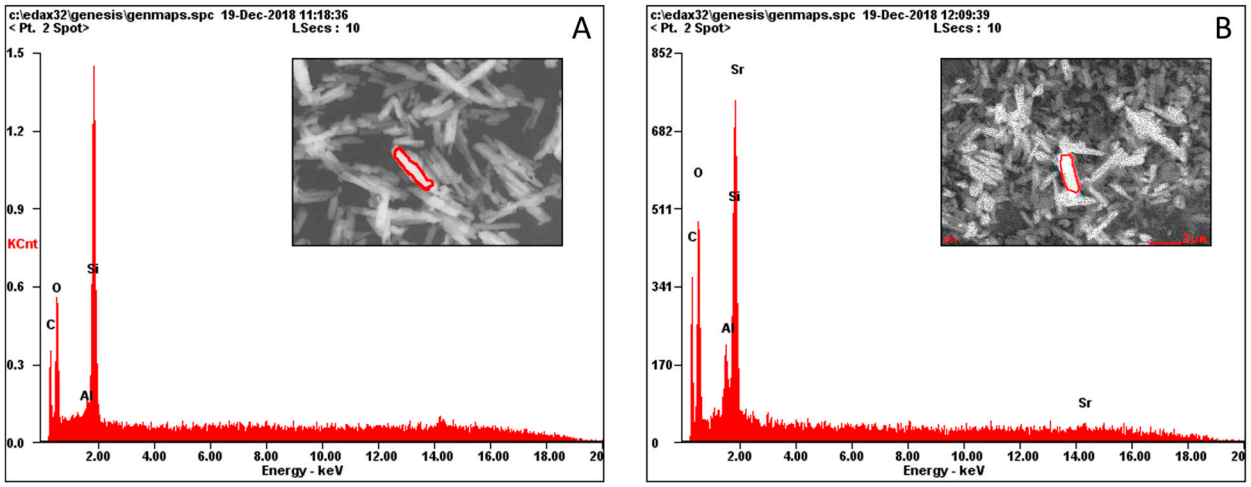

Figure 4. (**A**) The quantitative elemental analysis of the area selected in the inserts in Figure 4A,B. SrHNT shows the wt.% of carbon [C], aluminum [Al], silicon [Si], and oxygen [O] of HNT. The peak of Si is clearly seen. (**B**) The quantitative elemental analysis of the area selected in the inserts (4A) HNT and (4B) SrHNT show the wt.% of carbon [C], aluminum [Al], silicon [Si], oxygen [O], and strontium [Sr] of SrHNT.

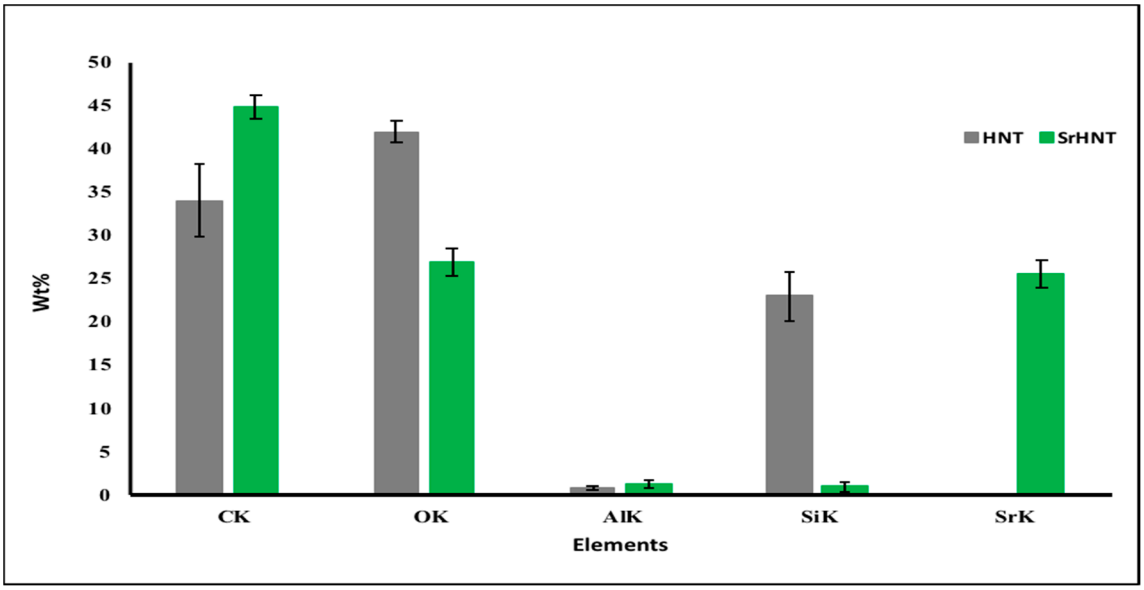

Figure 5. Quantitative wt.% of the elements present in HNT and SrHNT namely K shell of C, Al, Si, O, and Sr where $n = 5$. The error bars = standard deviation of the samples.

4.4. FTIR-ATR

To confirm the presence of Sr on HNTs, FTIR-ATR was conducted on the HNT samples, which provided the molecular fingerprint to compare the samples. The high spectral resolution data of the three samples can be seen in Figure 6A. Light in the infra-red region was absorbed, corresponding to specific bonds present in the samples. The absorption peaks on the inverted y-axis depict the percent of transmittance radiation in the sample.

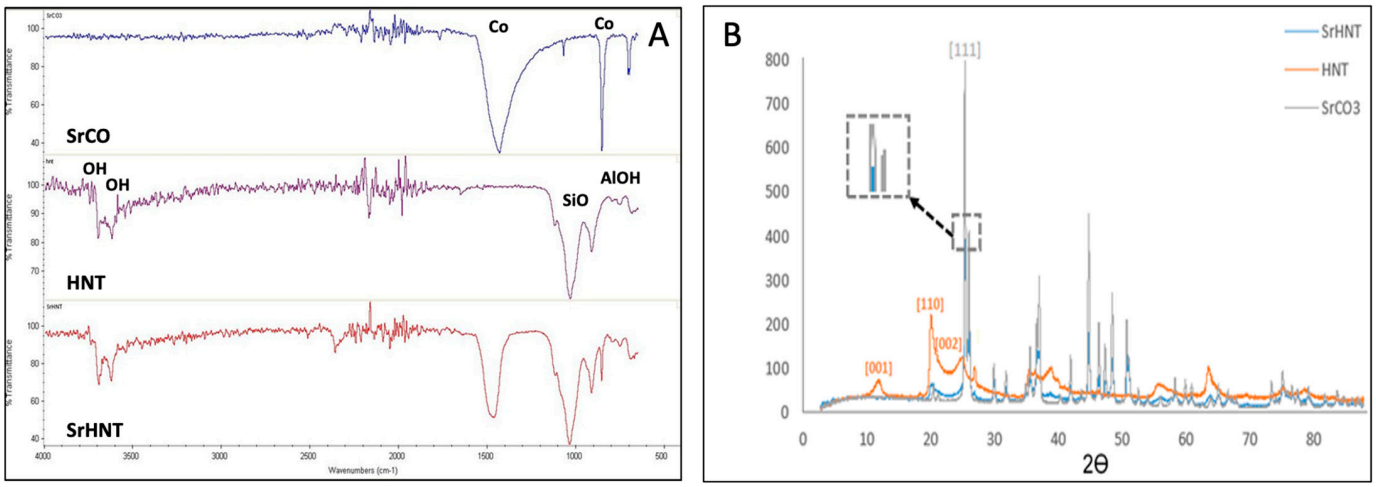

Figure 6. Elemental Analysis. (**A**) FTIR-ATR analysis of (—) $SrCO_3$ (—) HNT and (—) SrHNT (n = 3). (**B**) XRD graph image of HNT, $SrCO_3$, and SrHNT.

$SrCO_3$ has a strong peak at 1400 and 800 cm^{-1} depicting the -CO group. The position of the carbonyl group depends on the function of the molecule. The position of the carbonyl group here is characteristic of $SrCO_3$. For HNT, there is a distinct peak at 1040 cm^{-1} showing the -SiO group. There is a peak at 900 cm^{-1} showing the presence of the AlOH bond. Band peaks at 3100–3700 cm^{-1} are caused by -OH groups. The OH bond usually appears. These peaks are distinguishing factors for recognizing HNTs. For SrHNT, there are combinations of peaks at 3100–3700 cm^{-1}, 1400-800 cm^{-1}, and 3600–400 cm^{-1}. IR radiation has an effect, such that the higher the frequency is, the higher the wavelength will. SrHNT showed a distinct presence of Sr on HNT in the sample. FTIR results also showed that the coating could be a combination of Sr^{2+} ions and $SrCO_3$. The peaks show the CO bond along with the presence of HNT absorption peaks. The validity of $SrCO_3$ FTIR results was confirmed based on previously published data. The peaks on SrHNT confirmed the presence of HNTs and $SrCO_3$.

4.5. XRD Analysis

To further confirm the presence of Sr on HNT, XRD was used as some bonds are not visible through FTIR (Figure 6B). Since the wavelength of X-rays is on the atomic scale, this was the final tool to measure the accuracy of the composition of SrHNTs. XRD was used to compare the diffractions of HNT, $SrCO_3$, and SrHNT, as seen above in Figure 6B. HNTs have distinctive peaks at lattice structures 001, 110, and 002. There is a distinct peak of $SrCO_3$ at 111. Since the HNT is covered by Sr^{2-}, the crystal structure of SrHNT shows reduced peaks of HNT but the distinctive characteristic peak of $SrCO_3$. This last peak shows that SrHNTs were coated with strontium.

4.6. Viability and Cytotoxicity Testing for SrHNTs

A Live/Dead assay was performed to confirm the percentage of SrHNT that would provide a beneficial effect without harming the cells (Figure 7).

Two different SrHNT concentrations were tested on pre-osteoblast cells. NIH ImageJ software was used to count the cells. As seen in Figure 7, cells exposed to HNTs showed good viability on days 1 (95%), 3 (95.6%), 5 (95.67%), and 7 (95.9%) at lower concentrations. At higher HNT concentrations, the viability at days 1 (88.8%), 3 (88.9%), 5 (84.8%), and 7 (97.1%) was slightly different. Cells exposed to SrHNTs (at a concentration of 25 µg/mL) showed viability on days 1 (88.2%), 3 (91.47%), 5 (92.5%) and 7 (97.135) after exposure.

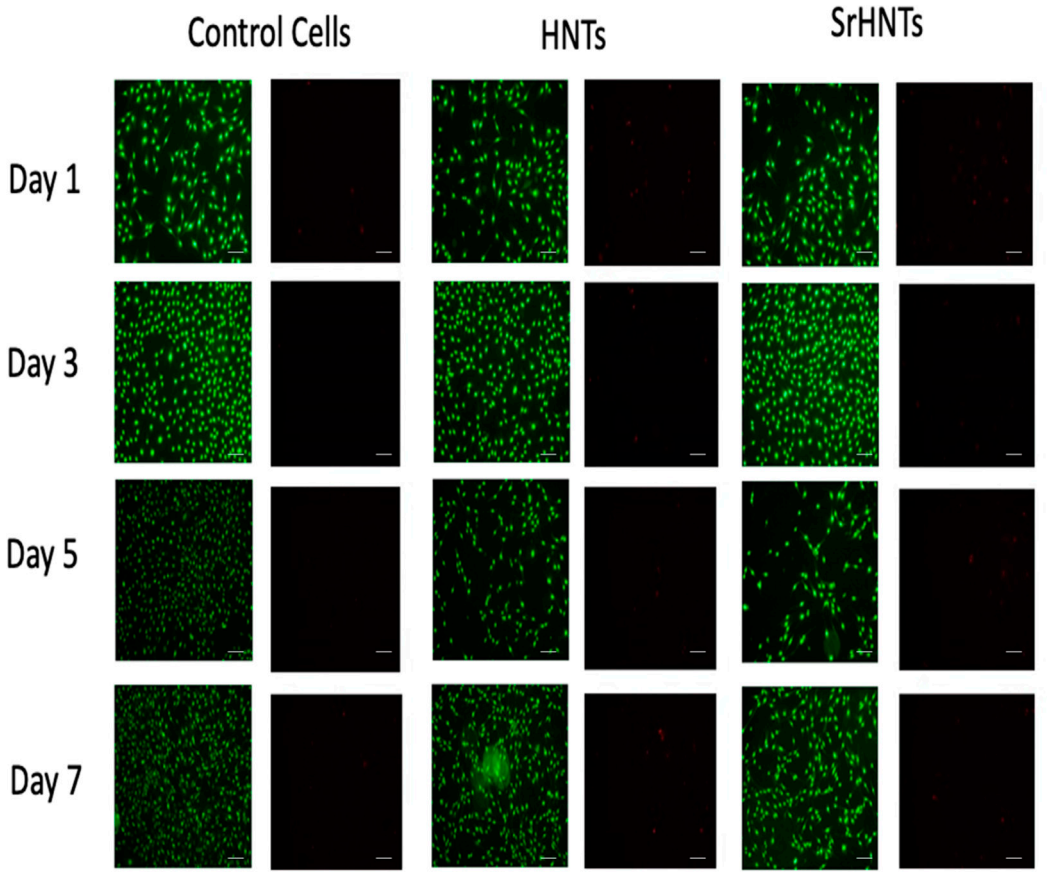

Figure 7. Live/Dead assay of two concentrations, 25 and 50 μg/mL of HNT and SrHNT, showing live cells in green images and dead cells in red for days 1, 3, 5, and 7.

At 50 μg/mL, SrHNTs showed an initial positive cellular response on day 1. By day 5, cell viability decreased (55.3%), and almost no live cells were seen by day 7 (Figure 7). No significant difference was revealed by the one-way ANOVA test performed using SPSS software.

Although no research has been published to show the absence of Sr's toxic effect, for the use of SrHNTs in biological systems, it was necessary to predict the concentration that could be used without hindering cell growth. These cytocompatibility tests were supported using Sr concentrations no higher than 25 μg/mL.

4.7. Proliferation Assay

The effect of different concentrations of HNTs and SrHNTs on pre-osteoblast cell proliferation was assessed over seven days, and the results are displayed in Figure 8. A higher cell count is equivalent to higher absorbance. Exposure to high concentrations of HNTs had a derogatory effect on proliferation compared to a lower HNT concentration. Cells exposed to SrHNTs proliferated. Further tests must be conducted to determine the impact of exposure on cells and for an extended period. The proliferation essay suggests that SrHNTs did not alter cell proliferation rate by a large degree and, with time in culture, could approach the rate of proliferation observed in control cells.

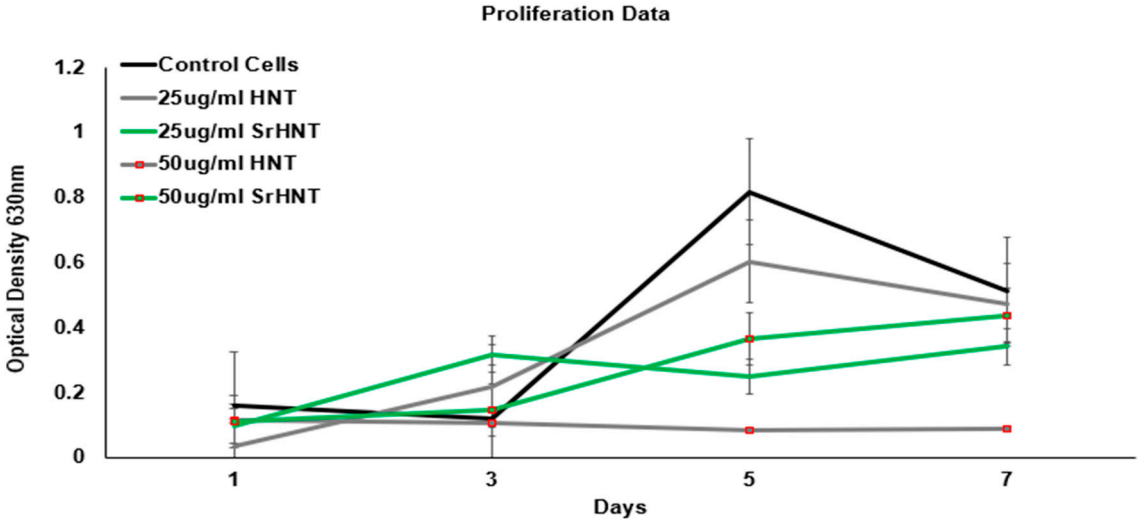

Figure 8. Graph showing proliferation of pre-osteoblast cells after exposure to two different concentrations of 25 and 50 µg/mL of HNT and SrHNT for days 1, 3, 5, and 7. Grey and green lines depict HNT and SrHNT, respectively. Marked lines represent high concentration lines. Error bars are standard deviations where $n = 3$.

As the graph shows, exposure to low (0.341 Å) and high (0.439 Å) concentrations of SrHNTs did not affect cell proliferation. However, exposure to a high concentration (0.09 Å) of HNTs had a more derogatory effect on proliferation than a low concentration (0.472 Å). As seen in Figure 8, there was no significant impact on cell proliferation damage after exposure of cells to a high concentration of SrHNTs. The rate of proliferation was higher in the case of SrHNTs. After being exposed to SrHNTs proliferated, cells exposed to high concentrations of HNTs showed a decline in proliferation. Further tests must be conducted to determine the effect of exposure on cells after an extended time. However, the assay showed that in the presence of SrHNTs, the cell proliferation rate did achieve a proliferation rate very similar to control cells over 7 days.

4.8. Bacterial Growth Rate

The effect of HNTs, SrHNTs, and gentamicin-loaded HNTs, SrHNTs, HNTSr (5 µg/mL) on the growth rate of *E. coli, S. aureus*, and *S. epidermis* was tested over 48 h (Figure 9A). Analysis of the data showed that HNTs have an inherent property that has some bactericidal or bacteriostatic effect on nosocomial bacteria. This was enhanced when HNTs were coated with Sr. When HNTs were loaded with gentamicin, it was released efficiently to inhibit bacterial growth. When HNTs were loaded and then coated with gentamicin, no bacterial growth was observed, showing the effectiveness of gentamicin release from HNTs.

SrHNT has some inherent quality that inhibits the bacterial growth rate. Coating HNTs with Sr before or after loading with drugs does not hinder drug release capacity, making them suitable carriers. The SrHNTs can serve as carriers for many drugs. When embedded in biomaterials such as CPC or hydrogels, this will be a better way to release the drugs in the implant, as research shows that loading drugs in carriers slow the release rate and prolong the duration of effects. Since SrHNT itself lowers the bacterial growth rate, it will help to reduce the chance of infection on the implant site for *S. aureus* (Figure 9B) and *S. epidermis* (Figure 9C) separately. SrHNT lowered the growth rate for all three bacteria compared to HNTs at a lower concentration.

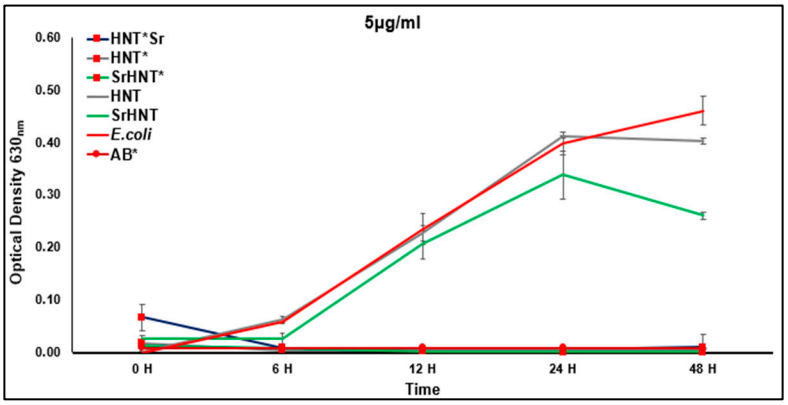

(**A**)

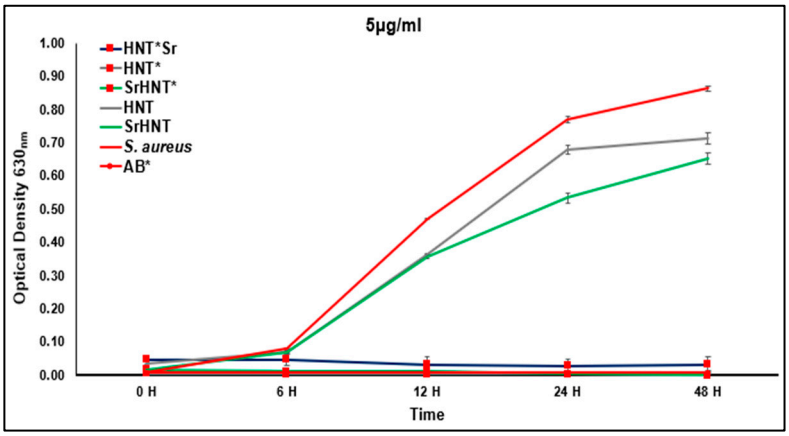

(**B**)

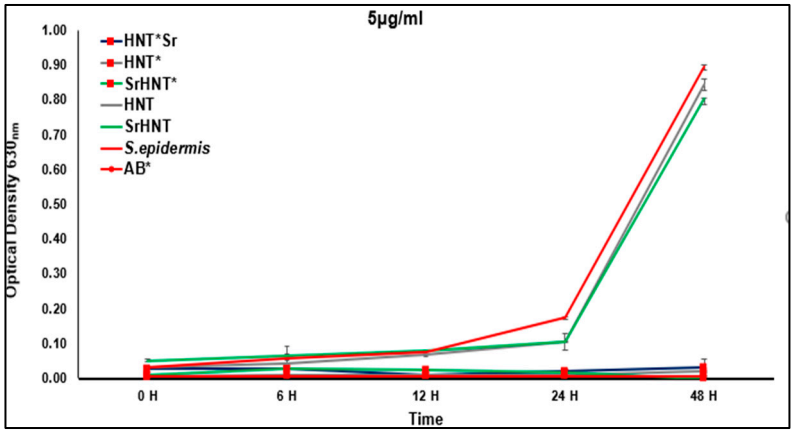

(**C**)

Figure 9. The pattern of bacterial growth over 24 h. Bacterial growth was tested based on the CSLI microtitration method. (**A**) *E. coli* (**B**) *S. aureus* (**C**) *S. epidermis*. The data are the averages of 3 different colonies. In this graph, the concentration of a sample of HNT, SrHNT, and Gentamicin loaded (5 µg) = HNTs *, SrHNTs *, and HNTSr *. The total reaction mixture was 100 µL. Error bars indicate the standard error of the mean.

5. Discussion

We successfully coated strontium on the surface of halloysite nanotubes. Several strategies exist for the metallization on HNT surfaces [45–50]. Existing fabrication methods include lengthy, multistep processes employing thermal decomposition [51,52], chemical reduction [53], and other techniques that use toxic reducing agents, costly chemicals, and require specialized equipment [44–51].

The solvothermal synthesis method is a chemical reaction occurring at high temperatures and pressure that changes the fundamental properties of the solvent [54–56]. The solvothermal process has two advantages. First, it is a one-step process with pH sensitivity and high photocatalytic activity. The disadvantages of such a method are the use of acids, bases, or other harsh chemicals as solvent or catalyst, specific requirements for oven for creating an atmosphere of high temperature; it is time-consuming and not cost-effective. In the silanization method, the surface of HNT is modified by using γ-aminopropyltriethoxysilane (APTES), which leads to Pd/NH2-HNT [44]. However, APTES is a toxic substance (MSDS health score = 3).

Therefore, the chemical is carefully used under a fume hood since it creates noxious odors that are destructive to the upper respiratory tract and mucous membranes. In addition, this compound acts on the kidneys, liver, and nerves; hence, APTES is used as an extreme precaution. The advantages of this method are that the surface property of the NH2-HNT is beneficial in improving the dispersion and loading of Pd, which can be uniformly distributed with smaller particle sizes. However, this result can lead to higher catalytic activity of the product. The disadvantages of this method are that it requires binding, which uses very toxic and harsh chemicals. In addition, it is a cumbersome and expensive process. In the dry sintering method, metal acetylacetonates are compounds often used to synthesize nanoparticles, metal catalysts, and NMR shift reagents [42,44]. The advantages of this process are that it is a simple process with more straightforward fabrication conditions, is environmentally safe, and does not require the use of any caustic material. The disadvantage of this method is that it is not very cost-effective, as it requires an energy source to keep the oven at 300 °C.

Our electrolysis method offers a facile process for depositing metal nanoparticles on the HNT surface. Metal nanoparticles (NPs), such as silver NPs, copper NPs, gold NPs, and others, can be directly deposited onto the surfaces of HNTs through this rapid, low-cost method. Furthermore, chemical processes that use toxic chemicals are not required, thus eliminating exposure to toxic chemicals and costs associated with the disposal of the resultant chemical waste. It offers a one-step and low-cost process for the fabrication of mHNTs. Sr was coated on the surface of HNTs without the need for harsh chemicals and did not produce any toxic waste.

The targeted application for our Sr-coated nanoclay is the remediation of a bone infection while promoting bone tissue formation. Surface adsorption of serum proteins facilitates bacterial adhesion and proliferation on the implant surface leading to biofilm formation [54]. A biofilm is a multicellular community of microbes forming on a solid surface or liquid–air interface. Microbes are densely packed within a self-assembled extracellular matrix that protects resident bacteria from various environmental agents in a biofilm [55,56]. As a result, they are much more resistant to antibiotics than the resident bacteria usually present in the human body. Often, a very resistant biofilm increases bacterial pathogenicity [54–56].

Our antibacterial tests showed that the SrHNTs have an inhibitory effect in bacterial growth. Gentamicin is a widely used antibiotic for treating infections because it can inhibit the growth of a broad spectrum of bacteria [57]. While effective, its major disadvantage is its low bioavailability after oral administration and poor cellular penetration [58]. In addition, when administrated systemically, gentamicin is excreted rapidly by the kidneys, resulting in a very low plasma half-life. This result then requires the administration of repeated doses leading to renal accumulation and nephrotoxicity [59,60]. Local antibiotic delivery to a site of bone infection can deliver an adequate dosage and avoid the need for prolonged administration of gentamicin and the resultant toxicity [61].

Furthermore, delivering antibiotics directly to the implant site rather than systemically through intravenous injection and prescription drugs could reduce the outbreak of resistant bacterial strains [57,58]. Furthermore, a biodegradable antibiotic carrier may result in a more significant release and obviate the need for removal; they are gradually replaced by ingrowing tissue [57]. Furthermore, the subsequent release of the antibiotic may occur dur-

ing the carrier's degradation phase; this could increase the antimicrobial efficacy compared to non-biodegradable carriers [7,57].

Several studies have shown the osteogenic activity of strontium [62–67]. Sr-coated HNTs were included within a biopolymer (3-polyhydroxybutyrate-co3-hydroxyvalerate) matrix [62]. This matrix showed increases in mechanical resistance and porosity, and a lack of cytotoxicity [62]. Strontium and selenium doped bioceramics were incorporated into polyacrylamide-carboxymethylcellulose hydrogels synthesized by free-radical polymerization. The composite hydrogel produces a supportive cell environment for MC3T3-E1 osteoblasts with enhanced cell proliferation and adhesion [63].

The composite also exhibited good alkaline phosphatase activity, suggesting its osteogenic potential [63]. Similar observations have been made in Sr/calcium phosphate composites [64–67]. Sr is also used in non-biological applications such as bio-glass [68–70].

An implantable scaffold significantly improves the osteogenic response and shortens recovery and healing in critical-sized bone defects is highly desired. Using MC 3T3 pre-osteoblasts, our cell culture studies showed that SrHNTs are cytocompatible and enhance cell proliferation. However, further studies on the osteogenic effects of SrHNTs are needed before any conclusion can be drawn. We have shown in previous studies that HNTs possess chemotactic, osteoconductive, and osteoinductive properties [39–41]. Therefore, we predict that antibiotic-doped SrHNTs added to calcium phosphate, or another supportive cell polymer can be used in a treatment that couples infection reduction while bone tissue is regenerated.

6. Conclusions

Bone defects may be caused by trauma, tumor, or infection, cause significant patient disability and suffering, and remain a significant clinical and socioeconomic problem. Therefore, developing a novel bone graft substitute that reduces bacterial infection and enhances bone regeneration is of clinical importance. We developed a facile method for coating the surfaces of halloysite nanotubes with strontium carbonate. The results showed that SrHNTs had a pronounced inhibitory effect on bacterial growth in both gram-positive and gram-negative strains. Furthermore, SrHNTs did not provoke a cytotoxic response and enhanced cell proliferation. Further studies are needed to explore SrHNT's osteoinductive capability. Nevertheless, the results support the potential of SrHNTs as a mechanism to combat bone infection and assist in tissue regeneration during bone defect repair.

Author Contributions: Conceptualization, A.E., D.K.M.; methodology, A.E.; software, A.E.; formal analysis, A.E., D.K.M.; data curation, A.E.; writing—original draft preparation, A.E.; writing, D.K.M.; supervision, D.K.M.; project administration, D.K.M.; funding acquisition, D.K.M. All authors have read and agreed to the published version of the manuscript.

Funding: The authors wish to acknowledge the funding assistance provided by the Center for Dental, Oral & Craniofacial Tissue & Organ Regeneration (C-DOCTOR) with the support of NIH NIDCR (U24DE026914).

Data Availability Statement: All relevant data are contained within the paper.

Conflicts of Interest: The authors declare no conflict of interest.

References

1. Campana, V.; Milano, G.; Pagano, E.; Barba, M.; Cicione, C.; Salonna, G.; Lattanzi, W.; Logroscino, G. Bone substitutes in orthopaedic surgery: From basic science to clinical practice. *J. Mater. Sci. Mater. Med.* **2014**, *25*, 2445–2461. [CrossRef] [PubMed]
2. Bauer, T.W.; Muschler, G.F. Bone graft materials. An overview of the basic science. *Clin. Orthop. Relat. Res.* **2000**, *371*, 10–27. [CrossRef]
3. Sanchez, C.J., Jr.; Ward, C.L.; Romano, D.R.; Hurtgen, B.J.; Hardy, S.K.; Woodbury, R.L.; Trevino, A.V.; Rathbone, C.R.; Wenke, J.C. Staphylococcus aureus biofilms decrease osteoblast viability, inhibits osteogenic differentiation, and increases bone resorption in vitro. *BMC Musculoskelet. Disord.* **2013**, *14*, 187. [CrossRef] [PubMed]
4. De Long, W.G., Jr.; Einhorn, T.A.; Koval, K.; McKee, M.; Smith, W.; Sanders, R.; Watson, T. Bone grafts and bone graft substitutes in orthopaedic trauma surgery: A critical analysis. *J. Bone Jt. Surg. Am.* **2007**, *89*, 649–658. [CrossRef]

5. Hatzenbuehler, J.; Pulling, T.J. Diagnosis and management of osteomyelitis. *Am. Fam. Physician* **2011**, *84*, 1027–1033. [CrossRef]
6. Tan, H.L.; Lin, W.T.; Tang, T.T. The use of antimicrobial impregnated PMMA to manage periprosthetic infections: Controversial issues and the latest developments. *Int. J. Artif. Organs.* **2012**, *35*, 832–839. [CrossRef]
7. Middleton, J.C.; Tipton, A.J. Synthetic biodegradable polymers as orthopedic devices. *Biomaterials* **2000**, *21*, 2335–2346. [CrossRef]
8. Tappa, K.; Jammalamadaka, U.; Mills, D.K. *Formulation and Evaluation of Nanoenhanced Antibacterial Calcium Phosphate Bone Cements*; Biomaterials, O., Webster, T., Li, B., Eds.; Springer: New York, NY, USA, 2018; pp. 85–108.
9. Han, S.Y.; Yoon, S.H.; Cho, K.H.; Cho, H.J.; An, J.H.; Ra, Y.S. Biodegradable polymer releasing antibiotic developed for drainage catheter of cerebrospinal fluid: In vitro results. *J. Korean Med. Sci.* **2005**, *20*, 297–301. [CrossRef]
10. Karageorgiou, V.; Kaplan, D. Porosity of 3D biomaterial scaffolds and osteogenesis. *Biomaterials* **2005**, *26*, 5474–5491. [CrossRef]
11. Burge, R.; Dawson-Hughes, B.; Solomon, D.H.; Wong, J.B.; King, A.; Tosteson, A. Incidence and economic burden of osteoporosis-related fractures in the United States, 2005–2025. *J. Bone Miner. Res.* **2007**, *22*, 465–475. [CrossRef]
12. Lane, N.E. Epidemiology, etiology, and diagnosis of osteoporosis. *Am. J. Obstet. Gynecol.* **2006**, *194* (Suppl. S2), S3–S11. [CrossRef]
13. Available online: https://www.piedmont.org/spine/conditions-diseases/spine-osteoporosis (accessed on 21 March 2020).
14. Knickman, J.R.; Snell, E.K. The 2030 problem: Caring for aging baby boomers. *Health Serv. Res.* **2002**, *37*, 849–884. [CrossRef]
15. Marie, P.J. Strontium ranelate: A novel mode of action optimizing bone formation and resorption. *Osteoporos. Int.* **2005**, *16*, S7–S10. [CrossRef] [PubMed]
16. Ammann, P. Strontium ranelate: A novel mode of action leading to renewed bone quality. *Osteoporos. Int.* **2005**, *16*, S11–S15. [CrossRef]
17. Panzavolta, S.; Torricelli, P.; Casolari, S.; Parrilli, A.; Fini, M.; Bigi, A. Strontium-substituted hydroxyapatite-gelatin biomimetic scaffolds modulate bone cell response. *Macromol. Biosci.* **2018**, *18*, e1800096. [CrossRef] [PubMed]
18. Bakker, A.D.; Zandieh-Doulabi, B.; Klein-Nulend, J. Strontium ranelate affects signaling from mechanically-stimulated osteocytes towards osteoclasts and osteoblasts. *Bone* **2013**, *53*, 112–119. [CrossRef] [PubMed]
19. Yang, F.; Yang, D.; Tu, J.; Zheng, Q.; Cai, L.; Wang, L. Strontium enhances osteogenic differentiation of mesenchymal stem cells and in vivo bone formation by activating Wnt/catenin signaling. *Stem Cells* **2011**, *29*, 981–991. [CrossRef] [PubMed]
20. Lode, A.C.; Heiss, G.; Knapp, J.; Thomas, B.; Nies, M.; Gelinsky, D.; Schumacher, M. Strontium-modified premixed calcium phosphate cements for the therapy of osteoporotic bone defects. *Acta Biomater.* **2018**, *65*, 475–485. [CrossRef]
21. Thormann, U.; Ray, S.; Sommer, U.; ElKhassawna, T.; Rehling, T.; Hundgeburth, M.; Henß, A.; Rohnke, M.; Janek, J.; Lips, K.S.; et al. Bone formation induced by strontium modified calcium phosphate cement in critical-size metaphyseal fracture defects in ovariectomized rats. *Biomaterials* **2013**, *34*, 8589–8598. [CrossRef]
22. Agrawal, S.; Kelkar, M.; De, A.; Kulkarni, A.R.; Gandhi, M.N. Surfactant free novel one-minute microwave synthesis, characterization and cell toxicity study of mesoporous strontium hydroxyapatite nanorods. *RSC Adv.* **2016**, *6*, 94921–94926. [CrossRef]
23. Bracci, B.; Torricelli, P.; Panzavolta, S.; Boanini, E.; Giardino, R.; Bigi, A. Effect of Mg^{2+}, Sr^{2+} and Mn^{2+} on the chemico-physical and in vitro biological properties of calcium phosphate biomimetic coatings. *J. Inorg. Biochem.* **2009**, *103*, 1666–1674. [CrossRef] [PubMed]
24. Boanini, E.; Gazzano, M.; Nervi, C.; Chierotti, M.R.; Rubini, K.; Gobetto, R.; Bigi, A. Strontium and zinc substitution in β-tricalcium phosphate: A d-ray diffraction, solid state NMR and ATR-FTIR study. *J. Funct. Biomater.* **2019**, *10*, 20. [CrossRef] [PubMed]
25. Lv, T.; Liang, W.; Li, L.; Cui, X.; Wei, X.; Pan, H.; Li, B. Novel calcitonin gene-related peptide/chitosan-strontium-calcium phosphate cement: Enhanced proliferation of human umbilical vein endothelial cells in vitro. *J. Biomed. Mat. Res. Pt B Appl. Biomat.* **2019**, *107*, 19–28. [CrossRef] [PubMed]
26. Shepherd, D.V.; Kauppinen, K.; Brooks, R.A.; Best, S.M. An in vitro study into the effect of zinc substituted hydroxyapatite on osteoclast number and activity. *J. Biomed. Mater. Res. A* **2014**, *102*, 4136–4141. [CrossRef]
27. Almeida, M.M.; Nani, E.P.; Teixeira, L.N.; Peruzzo, D.C.; Joly, J.C.; Napimoga, M.H.; Martinez, E.F. Strontium ranelate increases osteoblast activity. *Tissue Cell* **2016**, *48*, 183–188. [CrossRef]
28. Joussein, E.; Petit, S.; Churchman, J.; Theng, B.; Righi, D.; Delvaux, B. Halloysite clay minerals—A review. *Clay Miner.* **2005**, *40*, 383–426. [CrossRef]
29. Zhang, Y.; Tang, A.; Yang, H.; Ouyang, J. Applications and interfaces of halloysite nanocomposites. *Appl. Clay Sci.* **2015**, *119*, 8–17. [CrossRef]
30. Tarasova, E.; Naumenko, E.; Rozhina, E.; Akhatova, F.; Fakhrullin, R. Cytocompatibility and uptake of polycations-modified halloysite clay nanotubes. *Appl. Clay Sci.* **2015**, *119*, 21–30. [CrossRef]
31. Abdllayev, E.; Lvov, Y. Functional polymer clay nanotube composites with sustained release of chemical agents. *Prog. Poly. Sci.* **2013**, *38*, 1690–1719.
32. Deng, S.; Zhang, J.; Ye, L. Halloysite-epoxy nanocomposites with improved particle dispersion through ball mill homogenisation and chemical treatments. *Compos. Sci. Technol.* **2009**, *69*, 2497–2505. [CrossRef]
33. Wei, W.; Abdullayev, E.; Hollister, A.; Mills, D.; Lvov, Y.M. Clay nanotube/poly(methyl methacrylate) bone cement composites with sustained antibiotic release. *Macromol. Mater. Eng.* **2012**, *297*, 645–653. [CrossRef]
34. Santos, A.C.; Ferreira, C.; Veiga, F.; Ribeiro, A.J.; Panchal, A.; Lvov, Y.; Agarwal, A. Yuri Lvov, and Anshul Agarwal. Halloysite clay nanotubes for life sciences applications: From drug encapsulation to bioscaffold. *Adv. Colloid Interface Sci.* **2018**, *257*, 58–70. [CrossRef] [PubMed]

35. Lvov, Y.; Wang, W.; Zhang, L.; Fakhrullin, R. Halloysite clay nanotubes for loading and sustained release of functional compounds. *Adv. Mater.* **2016**, *28*, 1227–1250. [CrossRef] [PubMed]
36. Fizir, M.; Dramou, P.; Dahiru, N.S.; Ruya, W.; Huang, T.; He, H. Halloysite nanotubes in analytical sciences and in drug delivery: A review. *Microchim. Acta* **2018**, *185*, 389. [CrossRef] [PubMed]
37. Yue Li, Y.; Mills, D.K. Halloysite nanotubes as a potential chemotactic agent for bone repair. In Proceedings of the Orthopedic Research Society Meeting, Phoenix, Arizona, 8–11 February 2020.
38. Tappa, K.; Jammalamadaka, U.; Mills, D.K. Formulation and evaluation of nanoenhanced antibacterial calcium phosphate bone cements. In *Orthopedic Biomaterials*; Springer: Cham, Switzerland, 2017; pp. 85–108.
39. Jammalamadaka, U.; Tappa, K.; Mills, D. Osteoinductive calcium phosphate clay nanoparticle bone cements (CPCs) with enhanced mechanical properties. In Proceedings of the 2014 36th Annual International Conference of the IEEE Engineering in Medicine and Biology Society, Chicago, IL, USA, 26–30 August 2014; pp. 3921–3924.
40. Karnik, S.; Mills, D.K. Nanoenhanced hydrogel system with sustained release capabilities. *J. Biomed. Mater. Res. Part A* **2015**, *103*, 2416–2426. [CrossRef]
41. Karnik, S.; Jammalaka, U.; Tappa, K.; Mills, D.K. Performance evaluation of nanoclay enriched antimicrobial hydrogels for biomedical applications. *Heliyon* **2016**, *2*, e00072. [CrossRef] [PubMed]
42. Nicholson, J.C.; Weisman, J.A.; Boyer, C.J.; Wilson, C.G.; Mills, D.K. Dry sintered metal coating of halloysite nanotubes. *Appl. Sci.* **2016**, *6*, 265. [CrossRef]
43. Shu, Z.; Zhang, Y.; Yang, Q.; Yang, H. Halloysite nanotubes supported Ag and ZnO nanoparticles with synergistically enhanced antibacterial activity. *Nanoscale Res. Lett.* **2017**, *12*, 135. [CrossRef]
44. Zhang, Y.; He, X.; Ouyang, J.; Yang, H. Palladium nanoparticles deposited on silanized halloysite nanotubes: Synthesis, characterization and enhanced catalytic property. *Sci. Rep.* **2013**, *3*, 2948. [CrossRef]
45. Chen, S.; Li, J.; Zhang, Y.; Zhang, D.; Zhu, J. Effect of preparation method on halloysite supported cobalt catalysts for Fischer-Tropsch synthesis. *J. Nat. Gas Chem.* **2012**, *21*, 426–430. [CrossRef]
46. Liu, P.; Zhao, M. Silver nanoparticle supported on halloysite nanotubes catalyzed reduction of 4-nitrophenol (4-NP). *Appl. Surf. Sci.* **2009**, *255*, 3989–3993. [CrossRef]
47. Abdullayev, E.; Sakakibara, K.; Okamoto, K.; Wei, W.; Ariga, K.; Lvov, Y. Natural tubule clay template synthesis of silver nanorods for antibacterial composite coating. *Am. Chem. Soc. Appl. Mater. Interfaces* **2011**, *3*, 4040–4046. [CrossRef] [PubMed]
48. Tang, X.; Li, L.; Shen, B.; Wang, C. Halloysite-nanotubes supported FeNi alloy nanoparticles for catalytic decomposition of toxic phosphine gas into yellow phosphorous and hydrogen. *Chemosphere* **2013**, *91*, 1368–1373. [CrossRef] [PubMed]
49. Vinokurov, V.A.; Stavitskaya, A.V.; Chudakov, Y.A.; Ivanov, E.V.; Shrestha, L.K.; Ariga, K.; Darrat, Y.A.; Lvov, Y.M. Formation of metal clusters in halloysite clay nanotubes. *Sci. Technol. Adv. Mater.* **2017**, *18*, 147–151. [CrossRef] [PubMed]
50. Massaro, M.; Colletti, C.G.; Lazzara, G.; Milioto, S.; Note, R.; Riela, S.J. Halloysite nanotubes as support for metal-based catalysts. *J. Mater. Chem. A* **2017**, *5*, 13276–13293. [CrossRef]
51. Markowska, K.; Grudniak, A.M.; Wolska, K.I. Silver nanoparticles as an alternative strategy against bacterial biofilms. *Acta Biochim. Pol.* **2013**, *60*, 523–530. [CrossRef]
52. Rezazadeh, T.; Khan, M.D.; Riche, K.; Lvov, Y.M.; Stavisky, A.V.; Wiley, J.B. Rapid and controlled in situ growth of noble metal nanostructures within halloysite clay nanotubes. *Langmuir* **2017**, *33*, 13051–13059.
53. Reddy, N.S.G.; Rao, K.M.; Park, S.Y.; Kim, T.; Chung, I. Fabrication of aminosilanized halloysite based floating biopolymer composites for sustained gastro retentive release of curcumin. *Macromol. Res.* **2019**, *27*, 490–496. [CrossRef]
54. Donlan, R.M. Biofilms: Microbial life on surfaces. *Emerg. Infect. Dis.* **2002**, *8*, 881–890. [CrossRef]
55. Khatoon, Z.; McTiernan, C.D.; Suuronen, E.J.; Mah, T.F.; Alarcon, E. Bacterial biofilm formation on implantable devices and approaches to its treatment and prevention. *Heliyon* **2018**, *4*, e01067. [CrossRef]
56. Paharik, A.E.; Horswill, A.R. The staphylococcal biofilm: Adhesins, regulation, and host response. *Microbiol. Spectr.* **2016**, *4*, 529–566. [CrossRef] [PubMed]
57. Lucke, M.; Wildemann, B.; Sadoni, S.; Surke, C.; Schiller, R.; Stemberger, A.; Raschke, M.; Haas, N.P.; Schmidmaier, G. Systemic versus local application of gentamicin in prophylaxis of implant-related osteomyelitis in a rat model. *Bone* **2015**, *36*, 770–778. [CrossRef]
58. McMillan, D.J.; Lutton, C.; Rosenzweig, N.; Sriprakash, K.S.; Goss, B.; Stemberger, M.; Schuetz, M.A.; Steck, R. Prevention of Staphylococcus aureus biofilm formation on metallic surgical implants via controlled release of gentamicin. *J. Biomed. Sci. Eng.* **2011**, *4*, 535–542. [CrossRef]
59. Aviv, M.; Berdicevsky, I.; Zilberman, M. Gentamicin-loaded bioresorbable films for prevention of bacterial infections associated with orthopedic implants. *J. Biomed. Mater. Res. A* **2007**, *83*, 10–19. [CrossRef] [PubMed]
60. Lopez-Novoa, J.M.; Quiros, Y.; Vicente, L.; Morales, A.I.; Lopez-Hernandez, F.J. New insights into the mechanism of aminoglycoside nephrotoxicity: An integrative point of view. *Kidney Int.* **2011**, *79*, 33–45. [CrossRef]
61. Saleh, P.; Abbasalizadeh, S.; Rezaeian, S.; Naghavi-Behzad, M.; Piri, R.; Pourfeizi, H.H. Gentamicin-mediated ototoxicity and nephrotoxicity: A clinical trial study. *Niger. Med. J.* **2016**, *57*, 347–352. [CrossRef]
62. Schmidmaier, G.; Lucke, M.; Wildemann, B.; Haas, N.P.; Raschke, M. Prophylaxis and treatment of implant-related infections by antibiotic-coated implants: A review. *Injury* **2006**, *37*, S105–S112. [CrossRef]

63. Buffa, S.; Bonini, M.; Ridi, F.; Severi, M.; Losi, P.; Volpi, S.; Al Kayal, T.; Soldani, G.; Baglioni, P. Design and characterization of a composite material based on Sr(II)-loaded clay nanotubes included within a biopolymer matrix. *J. Coll. Interface Sci.* **2015**, *448*, 501–507. [CrossRef]
64. Sarina, N.; Kurakulab, M.; Singha, K.J.; Kumar, A. Strontium and selenium doped bioceramics incorporated polyacrylamide-carboxymethylcellulose hydrogel scaffolds: Mimicking key features of bone regeneration. *J. Asian Ceramic Soc.* **2021**, *9*, 531–548. [CrossRef]
65. Martín-Del-Campo, M.; Sampedro, J.G.; Flores-Cedillo, M.L.; Rosales-Ibañez, R.; Rojo, L. Bone regeneration induced by strontium folate loaded biohybrid scaffolds. *Molecules* **2019**, *24*, 1660. [CrossRef]
66. Rojo, L.; Radley-Searle, S.; Fernandez-Gutierrez, M.; Rodriguez-Lorenzo, L.M.; Abradelo, C.; Deb, S.; Roman, J.S. The synthesis and characterization of strontium and calcium folates with potential osteogenic activity. *Mater. Chem. B* **2015**, *3*, 2708–2713. [CrossRef] [PubMed]
67. Thormann, U.; Ray, S.; Sommer, U.; ElKhassawna, T.; Rehling, T.; Hundgeburth, M.; Henß, A.; Rohnke, M.; Janek, J.; Lips, K.S.; et al. Bone formation induced by strontium modified calcium phosphate cement in critical-size metaphyseal fracture defects in ovariectomized rats. *Biomat* **2019**, *34*, 8589–8598.
68. Shi, H.; Zeng, S.; Liu, X.; Yu, T.; Zhou, C. Effects of strontium doping on the degradation and Sr ion release behaviors of α-tricalcium phosphate bone cement. *J. Am. Chem. Soc.* **2017**, *101*, 502–508. [CrossRef]
69. Cui, X.; Zhang, Y.; Wang, J.; Huang, C.; Wang, Y.; Yang, H.; Liu, W.; Wang, T.; Wang, D.; Wang, G.; et al. Strontium modulates osteogenic activity of bone cement composed of bioactive borosilicate glass particles by activating Wnt/β-catenin signaling pathway. *Bioact. Mater.* **2020**, *5*, 334–347. [CrossRef]
70. Saeid, K.; Montazerian, M.; Fiume, E.; Baino, F. Multiple and promising applications of strontium (Sr)-containing bioactive glasses in bone tissue engineering. *Front. Bioeng. Biotechnol.* **2019**, *7*, 161.